

Phase Fluctuations in Bose-Einstein Condensates

D. Hellweg¹, S. Dettmer¹, P. Ryytty¹, J. J. Arlt¹, W. Ertmer¹, K. Sengstock¹, D. S. Petrov^{2,3}, G. V. Shlyapnikov^{2,3,4}, H. Kreutzmann⁵, L. Santos⁵, and M. Lewenstein⁵

¹ Institut für Quantenoptik, Universität Hannover, Welfengarten 1, 30167 Hannover, Germany

² FOM Institute for Atomic and Molecular Physics, Kruislaan 407, 1098 SJ Amsterdam, The Netherlands

³ Russian Research Center Kurchatov Institute, Kurchatov Square, 123182 Moscow, Russia

⁴ Laboratoire Kastler Brossel, Ecole Normale Supérieure, 24 rue Lhomond, 75231 Paris Cedex 05, France

⁵ Institut für Theoretische Physik, Universität Hannover, Appelstraße 2, 30167 Hannover, Germany

The date of receipt and acceptance will be inserted by the editor

Abstract We demonstrate the existence of phase fluctuations in elongated Bose-Einstein Condensates (BECs) and study the dependence of those fluctuations on the system parameters. A strong dependence on temperature, atom number, and trapping geometry is observed. Phase fluctuations directly affect the coherence properties of BECs. In particular, we observe instances where the phase coherence length is significantly smaller than the condensate size. Our method of detecting phase fluctuations is based on their transformation into density modulations after ballistic expansion. An analytic theory describing this transformation is developed.

PACS: 03.75.Fi, 32.80.Pj, 05.30.Jp

1 Introduction

Bose-Einstein condensates of weakly interacting gases, such as alkali atom vapours, constitute very well controllable macroscopic quantum systems. For extremely low temperatures ($T \rightarrow 0$) the condensate is well described by an effective macroscopic single particle wavefunction, occupied by millions of atoms [1]. The corresponding macroscopic phase is related to many fascinating properties of BEC such as its coherence, superfluidity, and effects known from superconductivity as the Josephson effect. In particular, the coherence properties are essential for very promising applications of BEC such as matter wave interferometry [2,3,4,5,6,7,8] or atom lasers [9] which rely on BEC as a source of coherent matter waves. The phase coherence of condensates was shown by imaging the interference pattern of two independent condensates which were brought to overlap [2]. Also using an interference technique it has been found that a trapped BEC has a uniform spatial phase [3] and therefore the coherence length is just limited by the size of the condensate. This result has also been obtained by

measuring the momentum distribution in the radial direction of a cigar shaped condensate by a spectroscopic technique [10]. These experiments have focused on the coherence properties of almost pure condensates, prepared at temperatures well below the critical temperature. The temperature dependence of the coherence of a BEC was studied in a 'double slit' experiment where an atom laser beam was extracted from a cigar shaped BEC at different radial positions [4]. A reduction of interference fringe visibility was observed for increasing temperature with the interference pattern being reproducible and thus indicating that the relative phase of the condensate fraction was not fluctuating randomly.

Even though the uniform spatial phase of a condensate has been confirmed in several experiments, it is not an obvious or even general property of BEC at finite temperature. The 'fragmentation' into independent condensates with randomly fluctuating relative phase was often discussed in the context of the nucleation process of a condensate [11]. There, the equilibrium state of the system was assumed to be a 'pure' condensate without phase fluctuations. However, before the condensate is completely formed phase fluctuations between different regions of the condensate are expected even though density fluctuations are suppressed. But also for the equilibrium state of a quantum system it is expected that low-dimensional (1D and 2D) quantum gases differ qualitatively from the 3D case with respect to statistical and phase correlation properties [12,13,14]. Low-dimensional quantum degenerate gases, where the trap energy-level spacing is larger than the interaction energy between atoms, have been experimentally realized in atomic hydrogen [15], Sodium [16], and Lithium [17] but phase correlation properties have not yet been experimentally investigated. Recently, it was shown theoretically [18] that for very elongated condensates phase fluctuations can be pronounced already in the equilibrium state of the usual 3D ensemble, where density fluctuations are suppressed. This was experimentally and theoretically

investigated in [19]. The phase coherence length in this case can be much smaller than the axial size of the sample.

In this paper we present detailed experimental and theoretical studies of phase fluctuations in elongated BEC. The dependence on the trapping geometry, temperature, and the number of condensed atoms is investigated. We demonstrate that the spatial phase of the condensates undergoes random fluctuations with an average value determined by the system parameters. In particular, our measurements show that the average phase fluctuations increase with tighter radial confinement. Thus, they are especially pronounced for very elongated geometries as are used to study the transition from 3D to 1D degenerate quantum gases [16, 19].

BEC has recently been achieved in elongated micro-circuit geometries in which radial trapping frequencies of tens of KHz or even MHz are possible [20]. Since this is more than an order of magnitude bigger than the radial frequencies at which we have observed phase fluctuations our results should be especially relevant for these systems. Phase fluctuations should also be considered if tight confinement waveguides are used for BECs [8] or guided atom lasers beams, even though our results directly apply only to the equilibrium state of the system.

Note, that phase fluctuations lead to a broadening of the momentum distribution, which is the Fourier transform of the single particle correlation function, defining the coherence length. Therefore, only in the absence of phase fluctuations, a BEC constitutes a state where ultimate control over the motion and position of atoms, limited only by Heisenberg's uncertainty relation, is achieved.

Fluctuations of the phase of a Bose condensate are due to thermal excitations and always appear at finite temperature. Their experimental characterization constitutes a test of many-body theories at finite temperature. If the wavelength of these excitations is smaller than all dimensions of the condensate they have a 3D character and do not lead to pronounced phase fluctuations. In elongated condensates however, low energy *axial* excitations have wavelengths larger than the *radial* size of the sample and therefore acquire a pronounced 1D behaviour leading to axial phase fluctuations, although density fluctuations of the equilibrium state are still suppressed. The coherence properties can be significantly altered as compared with previous observations. In particular, the coherence length, i.e. the distance at which the single particle correlation function falls to e^{-1} , can be much smaller than the axial size of the condensate. This is not in contradiction to previous coherence measurements since they were performed in rather spherical traps [3], in the radial direction of cigar shaped condensates [4, 10], and at low temperature [3, 10].

Our method to study phase fluctuations is based on ballistic expansion. We show that the original phase distribution is mapped into the density distribution during time-of-flight. The density modulations after ballistic ex-

pansion are a direct measure of the original phase fluctuations of the trapped condensate.

The paper is organized as follows. It starts with a theoretical discussion of phase fluctuations including a detailed explanation of our analytic theory [19] for the appearance of density modulations in the ballistic expansion. Then we present our experimental studies demonstrating the existence of phase fluctuations in BECs and investigating their dependence on system parameters. Finally, alternative methods to study phase fluctuations are discussed, including simulations of the interference of phase fluctuating condensates.

2 Theoretical description

2.1 Phase fluctuating condensates in elongated 3D traps

In a standard equilibrium situation in 3D traps the fluctuations of density and phase of the Bose-Einstein condensate are only important in a narrow temperature range near the BEC transition temperature T_c (critical fluctuations). Outside this region, the fluctuations are suppressed and the condensate is phase coherent. This picture precludes the interesting physics of phase-fluctuating condensates, which is present in 2D and 1D systems (see [12, 13] and refs. therein).

In the Thomas-Fermi regime (see e.g. [1]), when the nonlinear mean field interaction energy dominates the kinetic energy, the situation can change for elongated BECs [18]. While density fluctuations in equilibrium will remain suppressed due to their energetic cost, the situation can be different for the phase fluctuations. In particular, the axial phase fluctuations can manifest themselves even at temperatures far below T_c . Then, as the density fluctuations are suppressed, the equilibrium state of the system becomes a *condensate with fluctuating phase* (quasicondensate) similar to that in 1D trapped gases [12]. Decreasing T gradually reduces the phase fluctuations.

2.2 Description of the fluctuating phase

In this section we describe the phase fluctuations along the lines of Ref. [18]. Let us consider a BEC at $T = 0$ in the Thomas-Fermi regime, where the mean-field (repulsive) interparticle interaction greatly exceeds the radial (ω_ρ) and axial (ω_x) trap frequencies. The density profile of the zero-temperature condensate has the well-known shape $n_0(\rho, x) = n_{0m}(1 - \rho^2/R^2 - x^2/L^2)$, where $n_{0m} = \mu/g$ is the maximum condensate density, with μ being the chemical potential, $g = 4\pi\hbar^2 a/m$, m the atom mass, and $a > 0$ the scattering length. Under the condition $\omega_\rho \gg \omega_x$, the radial size of the condensate, $R = (2\mu/m\omega_\rho^2)^{1/2}$, is much smaller than the axial size $L = (2\mu/m\omega_x^2)^{1/2}$.

The phase fluctuations can be described by solving the Bogoliubov-de Gennes equations [21] describing elementary excitations of the condensate. One can write the total field operator of atoms as $\hat{\psi}(\mathbf{r}) = \sqrt{n_0(\mathbf{r})} \exp(i\hat{\phi}(\mathbf{r}))$, where $\hat{\phi}(\mathbf{r})$ is the operator of the phase, and the density fluctuations have been already neglected following the arguments discussed above. The single-particle correlation function is then expressed through the mean square fluctuations of the phase (see, e.g. [22]):

$$\langle \hat{\psi}^\dagger(\mathbf{r}) \hat{\psi}(\mathbf{r}') \rangle = \sqrt{n_0(\mathbf{r}) n_0(\mathbf{r}')} \exp\{-\langle [\delta\hat{\phi}(\mathbf{r}, \mathbf{r}')]^2 \rangle / 2\}, \quad (1)$$

with $\delta\hat{\phi}(\mathbf{r}, \mathbf{r}') = \hat{\phi}(\mathbf{r}) - \hat{\phi}(\mathbf{r}')$. The operator $\hat{\phi}(\mathbf{r})$ is given by (see, e.g., [23])

$$\hat{\phi}(\mathbf{r}) = [4n_0(\mathbf{r})]^{-1/2} \sum_j f_j^+(\mathbf{r}) \hat{a}_j + h.c., \quad (2)$$

where \hat{a}_j is the annihilation operator of the excitation with quantum number(s) j and energy ϵ_j , $f_j^+ = u_j + v_j$, and the u, v functions of the excitations are determined by the Bogoliubov-de Gennes equations.

The “low-energy” axial excitations (with energies $\epsilon_j < \hbar\omega_\rho$) have wavelengths larger than R and exhibit a pronounced 1D behavior. Hence, one expects that these excitations give the most important contribution to the long-wave axial fluctuations of the phase. The solution of the Bogoliubov-de Gennes equations for such low-energy axial modes gives the spectrum $\epsilon_j = \hbar\omega_x \sqrt{j(j+3)}/4$ [21], where j is a positive integer. The wavefunctions f_j^+ of these modes have the form

$$f_j^+(\mathbf{r}) = \sqrt{\frac{(j+2)(2j+3)gn_0(\mathbf{r})}{4\pi(j+1)R^2L\epsilon_j}} P_j^{(1,1)}\left(\frac{x}{L}\right), \quad (3)$$

where $P_j^{(1,1)}$ are Jacobi polynomials. Note that the contribution of the low-energy axial excitations to the phase operator (2) is independent of the radial coordinate ρ .

2.3 Numerical simulations

In order to simulate numerically the effect of phase fluctuations during the ballistic expansion of the condensate we replace the operators \hat{a}_j and \hat{a}_j^\dagger in Eq. (2) by complex Gaussian random variables α_j and α_j^* , with the correlation $\langle \alpha_j \alpha_{j'}^* \rangle = \delta_{jj'} N_j$, where N_j is the occupation number for the quasiparticle mode j for a given (small) temperature T . Such a random phase reproduces correctly the phase correlations, which for not too large $|x - x'|/L \leq 0.4$, behave as

$$\langle [\delta\hat{\phi}(x, x')]^2 \rangle_T = \delta_L^2 |x - x'|/L, \quad (4)$$

where the quantity δ_L^2 is given by

$$\delta_L^2(T) = 32\mu T / 15N_0(\hbar\omega_x)^2, \quad (5)$$

and $l_\phi = L/\delta_L^2$ can be interpreted as a phase coherence length. It is the distance at which the phase factor of the

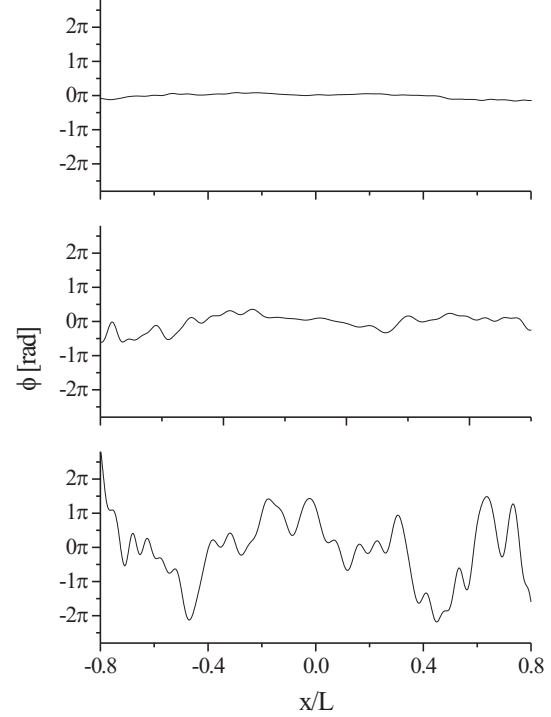


Fig. 1 Typical phase patterns for three different trap aspect ratios: $\lambda = 10$ (top), $\lambda = 100$ (middle), and $\lambda = 1000$ (bottom). For all cases $\omega_x = 2\pi \times 14$ Hz, $T = 0.6 T_c$, and $N = 2 \times 10^5$.

single-particle correlation function (Eq. 1) falls to its $1/e$ value. The condition $l_\phi/L = 1$ determines then a characteristic temperature $T_\phi = 15(\hbar\omega_x)^2 N_0 / 32\mu$, where N_0 is the number of condensed atoms. For $T_\phi < T_c$, which is the case for most of our measurements, one expects the regime of quasicondensation for the initial cloud in the temperature interval $T_\phi < T < T_c$ [18].

Figure 1 shows examples of simulated phase distributions for various trap geometries parameterized by the ratio of trapping frequencies $\lambda = \omega_\rho/\omega_x$. Whereas for a trap with $\lambda = 10$ the fluctuations are rather suppressed, the phase of the BEC fluctuates for a trap with $\lambda = 1000$ by more than 2π . This dramatically changes the properties of the condensate, especially in phase sensitive experiments.

The appearance of stripes in the process of ballistic expansion can be understood qualitatively as follows. As mentioned above, within the equilibrium state of a BEC in a magnetic trap the density distribution remains largely unaffected even if the phase fluctuates [18]. The reason is that the mean-field interparticle interaction prevents the transformation of local velocity fields provided by the phase fluctuations into modulations of the density. However, after switching off the external trap, the mean-field interaction rapidly decreases and the axial velocity field is then converted into a particular density distribution. We have performed numerical simulations

of the 3D Gross-Pitaevskii equation (GPE) to understand quantitatively how phase fluctuations lead to the build up of stripes in the density distribution. We assumed that initially (just before opening of the trap) the condensate had an equilibrium density profile, which has been calculated using the standard imaginary evolution of the GP equation. We have imprinted on it a random fluctuating phase $\phi(x)$, as described above, and evolved the condensate in free space.

2.4 Analytic results

Alternatively, the appearance of the stripes and their statistical properties can be described analytically using the self-similar solutions of the GP equation valid for the expanding cloud in the Thomas-Fermi regime (see e.g. [24]). In the following we shall assume for simplicity that the condensate is an infinite cylinder. This assumption is justified since the typical size of the excitations is much smaller than the axial size of the condensate. Therefore, at the end of the calculation, the unperturbed density will be substituted by the corresponding local density. In this way, the condensate without initial fluctuations evolve according to the self-similar solution

$$\psi = \frac{\sqrt{n_0}}{b_\rho^2(t)} e^{i\phi_0}, \quad (6)$$

where $b_\rho^2(t) = 1 + \omega_\rho^2 t^2$, $\phi_0 = \frac{m}{2\hbar} \frac{b_\rho}{b_\rho} \rho^2$, ρ is the radial coordinate, and n_0 is the Thomas-Fermi density profile. The equations which determine the ballistic expansion in presence of fluctuations can be obtained by linearizing around the self-similar solution, for the density $n_0 + \delta n$, and the phase $\phi_0 + \phi$. Introducing this expressions in the corresponding Gross-Pitaevskii equation, we obtain:

$$\dot{\delta n} = \frac{1}{b_\rho^2} \hat{O} \phi - \frac{\hbar \nabla_x^2 (n_0 \phi)}{m}, \quad (7)$$

$$n_0 \dot{\phi} = \frac{g n_0 \delta n}{\hbar b_\rho^2} + \frac{1}{4b_\rho^2} \hat{O} \left(\frac{\delta n}{n_0} \right) - \frac{\hbar \nabla_x^2 \delta n}{4m}, \quad (8)$$

where $\hat{O} = -(\hbar/m)(\nabla_{\rho'} n_0 \cdot \nabla_{\rho'} + n_0 \nabla_{\rho'}^2)$, and $\rho' = \rho/b_\rho$. By combining Eqs. (7) and (8), we obtain:

$$\dot{\delta n} - \frac{g n_0 \nabla_x^2 \delta n}{m b_\rho^2} + \frac{\hbar^2 \nabla_x^4 \delta n}{4m^2} = \frac{\partial}{\partial t} \left(\frac{\hat{O} \phi}{b_\rho^2} \right) + \frac{\hbar}{4b_\rho^2 m} \nabla_x^2 \hat{O} \frac{\delta n}{n_0}. \quad (9)$$

The last term at the rhs of Eq. (9) can be neglected if $\mu/\hbar\omega_\rho \gg 1$ (i.e. in the Thomas-Fermi limit). The third term in the lhs of the equation (quantum pressure term) is for short times smaller than the second one on the lhs, but becomes comparable with it for times $t \sim (1/\omega_\rho) \sqrt{\mu m/\hbar^2 k^2}$. This becomes an important point as discussed below. Averaging over the radial profile (employing the expansion in powers of ρ as discussed in Ref.

[21]), we end up with the equation:

$$\ddot{\delta n} - \frac{\mu}{2m b_\rho^2} \nabla_x^2 \delta n + \frac{\hbar^2}{4m^2} \nabla_x^4 \delta n = 0. \quad (10)$$

Expanding into the Bogoliubov eigenmodes of the system, then

$$\hbar^2 \delta \ddot{n}_k + \epsilon_k^2(t) \delta n_k = 0 \quad (11)$$

where

$$\epsilon_k(t) = \sqrt{\frac{\mu \hbar^2 k^2}{2m b_\rho^2} + \frac{\hbar^4 k^4}{4m^2}}, \quad (12)$$

is the Bogoliubov spectrum.

For short times $\omega_\rho t \lesssim 1$ the phonon part of the spectrum is dominant, i.e. $\epsilon_k(t) \simeq \sqrt{\frac{\mu \hbar^2 k^2}{2m b_\rho^2}}$. The resulting equation can be solved in terms of hypergeometric functions. For larger times, the free particle part of the spectrum dominates, i.e. $\epsilon_k = \frac{\hbar^2 k^2}{2m}$, and the equation can be solved in terms of Bessel functions. The two regimes may be matched, using the asymptotic expansions of both hypergeometric and Bessel functions. In this way, we end up with the analytic expression for the relative density fluctuations

$$\frac{\delta n}{n_0} = 2 \sum_j \tau^{-(\epsilon_j/\hbar\omega_\rho)^2} \sin \left(\frac{\epsilon_j^2 \tau}{\mu \hbar \omega_\rho} \right) \hat{\phi}_j, \quad (13)$$

where the sum extends over the axial modes $\epsilon_j = \hbar\omega_x \sqrt{j(j+3)}/4$, $\tau = \omega_\rho t$, and $\hat{\phi}_j$ is the contribution of the j -th mode to the phase operator in Eq. (2).

By substituting the operators by the corresponding c-numbers as discussed above, we have checked that the analytical expressions agree very well with the numerical results (see also Fig. 2).

2.5 Averages

From Eq.(13) one obtains a closed relation for the mean square density fluctuations σ^2 by averaging $(\delta n/n_0)^2$ over different realizations of the initial phase. Taking into account that $\langle (\alpha_j + \alpha_j^*)(\alpha_{j'} + \alpha_{j'}^*) \rangle / 4 = N_j \delta_{jj'} / 2$, then the mean square fluctuations are given by:

$$\left\langle \left(\frac{\delta n(x, t)}{n_0(x, t)} \right)^2 \right\rangle = \frac{T}{T_\phi} C(N_0, \omega_\rho, \omega_x, x, t)^2, \quad (14)$$

where

$$\begin{aligned} C(N_0, \omega_\rho, \omega_x, x, t)^2 = & \frac{1}{2} \sum_{j=1}^{\infty} \sin^2 \left(\frac{(j+3/2)^2}{4\alpha(1-(x/L)^2)} \right) e^{-\left(\frac{\omega_x}{\omega_\rho}\right)^2 \frac{(j+3/2)^2}{2} \ln(2\omega_\rho t)} \\ & \left(\frac{(j+2)(2j+3)}{j(j+1)(j+3)} \right) (P_j^{(1,1)} \left(\frac{x}{L} \right))^2, \end{aligned} \quad (15)$$

with $\alpha = \mu/\hbar\omega_x^2 t$.

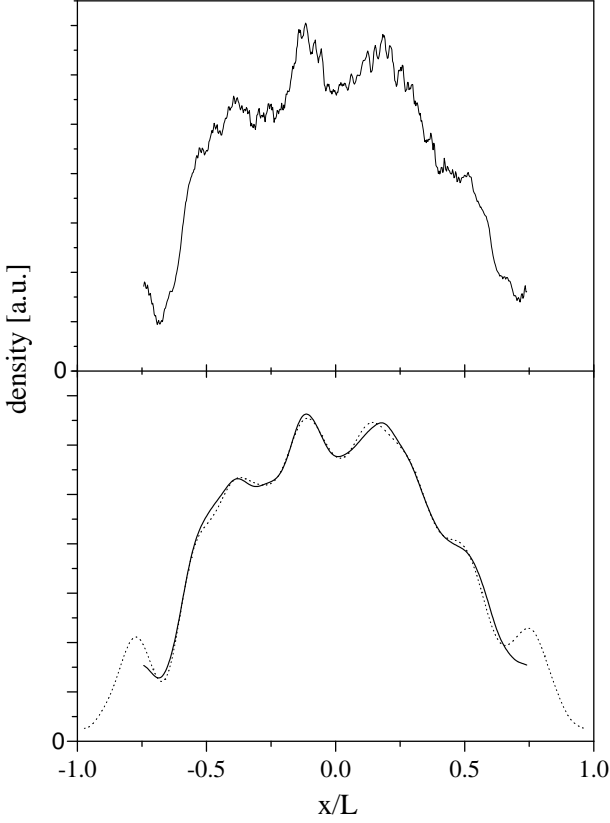


Fig. 2 Typical density profile after 25 ms time-of-flight. Top: numerical simulation without taking into account a limited experimental resolution. Bottom: numerical simulation (dotted line) compared with the analytic theory (solid line), both taking into account an experimental resolution of $\sigma = 3 \mu\text{m}$. All profiles were calculated for $\omega_x = 2\pi \times 14 \text{ Hz}$, $\omega_\rho = 2\pi \times 508 \text{ Hz}$, $N_0 = 2 \times 10^5$, and $T = 0.5 T_c$. For all the figures the same initial phase pattern was used.

Using the quasiclassical average $(P_j^{(1,1)}(x))^2 \simeq 4(1 - x^2)^{-3/2}/\pi j$ and transforming the sum over j into an integral, for the central part of the cloud ($x \approx 0$) we obtain

$$\left\langle \left(\frac{\delta n(0, t)}{n_0(0, t)} \right)^2 \right\rangle = \left(\frac{\sigma_{BEC}}{n_0} \right)^2 = \frac{T}{\epsilon T_\phi} \sqrt{\frac{\ln \tau}{\pi}} \left(\sqrt{1 + \sqrt{1 + \left(\frac{\hbar \omega_\rho \tau}{\mu \ln \tau} \right)^2}} - \sqrt{2} \right). \quad (16)$$

Note that Eq. (16) provides a direct relation between the observed density fluctuations and temperature, and thus can be used for thermometry at very low T .

This closed expression would provide an accurate description of the density fluctuations in the absence of any experimental limitation. However, in practice, the observation of the density fluctuations is limited by the spatial resolution of the experiment. This fact can be easily taken into account in the calculations by substituting $P_j^{(1,1)}(x/L)$ in Eq. (15) by the corresponding function

convoluted by a resolution function $\zeta(x) = e^{-x^2/\sigma^2}/\sqrt{\pi}\sigma$, where σ characterizes the experimental resolution (Fig. 2).

Other experimental limitations can be easily taken into account by following a similar procedure. In particular, a smoothing of the observed density ripples is produced if the laser that integrates the condensate column density in the absorption detection scheme is not exactly parallel to the density stripes. This effect can be easily incorporated into the calculations, by filtering the density distribution with a cut-off function in the Fourier spectrum of the form $\exp(ikRb_\rho(t)\theta) \sin(kRb_\rho(t)\theta)/kTb_\rho(t)\theta$, where θ is the angle between the laser and the density ripples. We return to this point in the experimental section.

3 Experimental Results

3.1 Experimental Setup

The experiment was performed with Bose-Einstein condensates of ^{87}Rb atoms in the $|F = 2, m_F = +2\rangle$ hyperfine ground state. As described previously [25, 26] we load a magneto-optical trap with a few times 10^9 atoms from a chirp slowed thermal beam. This is followed by a short period of subdoppler cooling and optical pumping into the desired magnetic sublevel. The atomic cloud is then loaded into an Ioffe-Pritchard type (cloverleaf) magnetic trap and finally adiabatically compressed to allow efficient rf evaporative cooling. The fundamental frequencies of our magnetic trap are $\omega_x = 2\pi \times 14 \text{ Hz}$ and $\omega_\rho = 2\pi \times 365 \text{ Hz}$ along the axial and radial direction, respectively. Due to the highly anisotropic confining potential with an aspect ratio $\lambda = \omega_\rho/\omega_x$ of 26 the condensates are already elongated along the horizontal x -axis.

In order to study the dependence of phase fluctuations on the trapping geometry we realized a wide range of radial confinement strengths. To allow for stronger radial confinement we used a holographically generated blue detuned Laguerre-Gauss mode (TEM_{01}^*) laser beam to form a combined magnetic and optical dipole potential trap [8]. In this combined trap BECs were produced in a two step evaporation procedure. The atoms were first cooled in the 'pure' magnetic trap to a temperature slightly above the transition temperature T_c . The optical dipole potential was then turned on adiabatically, and finally the desired temperature was achieved by rf evaporation in the combined potential. On the other hand less elongated condensates were produced by using a higher offset-field for the magnetic trap leading to a weaker radial confinement.

Our measurements were performed for an axial trap frequency of $\omega_x = 2\pi \times 14 \text{ Hz}$ and radial frequencies ω_ρ between $2\pi \times 138 \text{ Hz}$ and $2\pi \times 715 \text{ Hz}$ corresponding to aspect ratios λ between 10 and 51. After rf evaporative cooling to the desired temperature, we wait for 1 sec

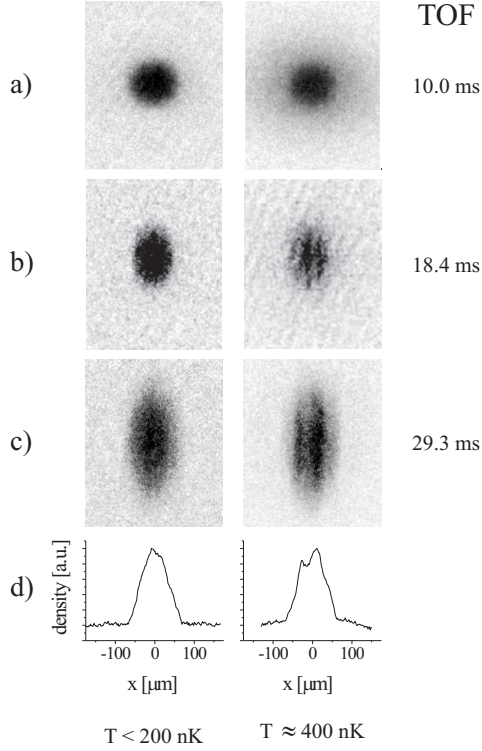


Fig. 3 (a)-(c): Absorption images for various times-of-flight and temperatures with $\omega_x = 2\pi \times 14$ Hz and $\omega_\rho = 2\pi \times 365$ Hz. (d): Density profiles for the clouds displayed in (c) integrated along the radial direction. In the case of $T < 200$ nK no thermal component was visible and the temperature was estimated to be $< T_c/2$.

(with rf 'shielding') to allow the system to reach an equilibrium state. We then switch off the trapping potential within 200μ s and wait for a variable time-of-flight before detecting the atomic cloud by resonant absorption imaging with the imaging axis perpendicular to the long axis of the trap.

3.2 Ballistic expansion measurements

Figure 3 shows typical images of the ballistically expanded clouds for various times-of-flight t and temperatures $T < T_c$. The usual anisotropic expansion of the condensate due to the elongated trapping geometry is clearly visible. The line density profiles reflect the parabolic shape of the BEC density distribution. As predicted by the theory, we also observe pronounced stripes in the density distribution. On average these stripes are more pronounced for high temperatures (right column of Fig. 3) and long times-of-flight [Fig. 3(c)] indicating the build-up of the stripes during the ballistic expansion.

3.3 Experimental characterization of phase fluctuations

In order to determine the dependence of phase fluctuations on the experimental conditions we study the for-

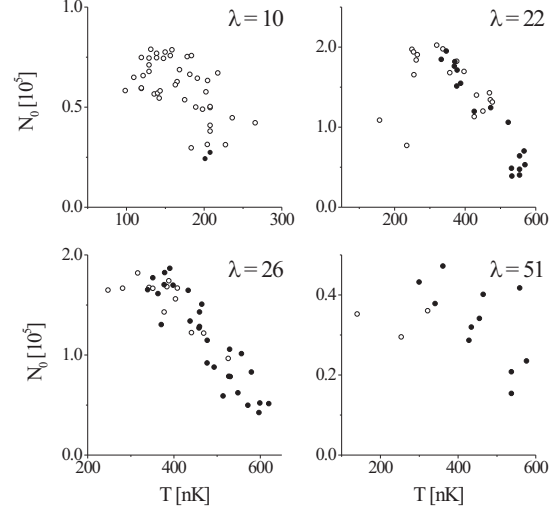


Fig. 4 Distribution of phase fluctuating condensates as a function of temperature and condensate number for four different trap geometries. White points indicate the absence of detectable structures ($\sigma_{\text{BEC}} < 1.5\sigma_T$), black points the existence of significant structures ($\sigma_{\text{BEC}} > 2\sigma_T$).

mation of the density modulations as a function of temperature and trapping geometry. All measurements were performed for times-of-flight between 18 ms and 25 ms. For a quantitative analysis we compare the observed density distribution with the Thomas-Fermi distribution expected for a condensate without fluctuations. For each image the observed density distribution was integrated along the radial direction [Fig. 3(d)] and then fitted by a bimodal function with the integrated parabolic Thomas-Fermi density distribution and a Gaussian for the thermal cloud. In Fig 3(d) we show the integrated density distribution close to the BEC region, thus the thermal component is hardly visible. The standard deviations of the experimental data from the fit were calculated in the central region of the BEC (half width of full size), σ_{BEC} , and in the thermal wings, σ_T . The standard deviation in the thermal wings characterizes our detection noise. To account for particle number changes the standard deviations were normalized to the fitted peak density n_0 .

Figure 4 shows the distribution of phase fluctuating condensates as a function of temperature and condensate number for various trap geometries. In this figure white points indicate the absence of detectable structures in the density distribution ($\sigma_{\text{BEC}} < 1.5\sigma_T$), whereas black points indicate that significant structures larger than the experimental noise level ($\sigma_{\text{BEC}} > 2\sigma_T$) were observed, i.e. the existence of phase fluctuations could be clearly detected. The temperature and particle number of each condensate were determined by 2D fits to the absorption images. The temperature was determined from the width of a Gaussian distribution fitted to the thermal wings, the corresponding condensate number from the integral

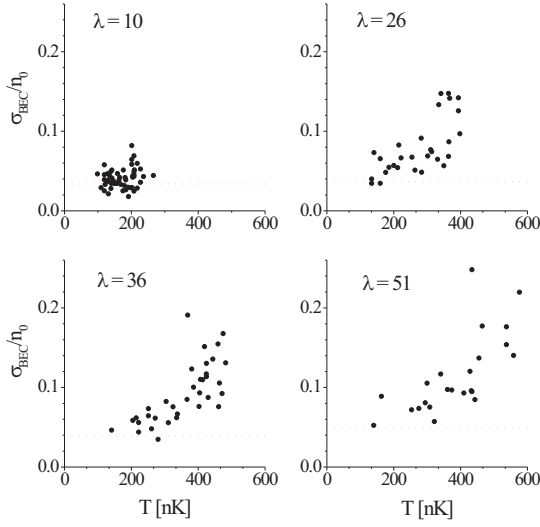


Fig. 5 Measurement of σ_{BEC}/n_0 versus temperature in four different trap geometries. The dotted lines represent the average detection noise σ_T/n_0 . All data was taken for $T < T_c$.

over the Thomas-Fermi part of a bimodal fit. The statistical uncertainty in the temperature determination is typically 15 % and less than 10 % for the particle numbers.

It is clearly visible in Fig. 4 that the number of condensates showing detectable phase fluctuations is increasing with the aspect ratio. Furthermore, the number of realizations without detectable phase fluctuations is growing for low temperatures and high particle numbers. Finally, there is no clear transition line between the two regimes. There is rather a broad region in which we observe both, condensates with and without detectable phase fluctuations indicating the statistical character of the phase fluctuations. Whereas for the weakest radial confinement with $\lambda = 10$, no significant structures were observed outside the close vicinity of the critical temperature, we detected pronounced phase fluctuations in a broad temperature range in the case of our tightest trap $\lambda = 51$ [Fig. 4]. According to Eq. 5 phase fluctuations can be reduced below any detection level for sufficiently low temperatures. However, for high aspect ratio traps this requires very low temperatures at high particle numbers in the condensate, making it experimentally difficult to access. For all traps the BECs were produced by evaporating in the final potential except in the case of the $\lambda = 10$ trap. This trap was realized by evaporating in the tighter $\lambda = 26$ trap and then adiabatically reducing the radial confinement. Thus the measurements show that by changing the trapping potential adiabatically we are able to decrease the amount of phase fluctuations. The dynamics of the appearance and disappearance of the phase fluctuations remains to be studied systematically in future work.

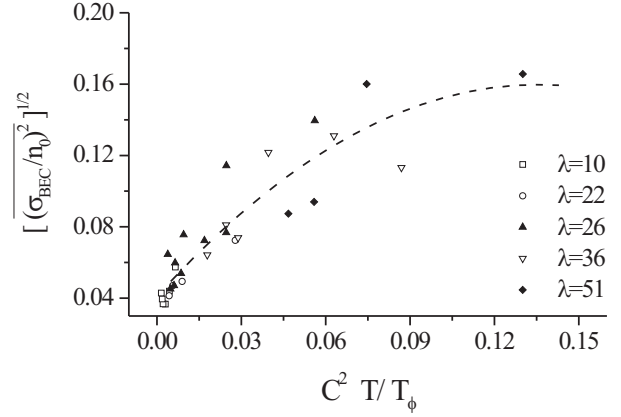


Fig. 6 Average standard deviation of the measured line densities $[(\sigma_{\text{BEC}}/n_0)^2]_{\text{exp}}^{1/2}$ as a function of temperature. The temperature-axis is scaled according to the expected dependence on the other experimental parameters (Eq. 14). The dashed line is a fit of a square root function to the data reflecting the theoretical expected dependence.

Figure 5 shows the temperature dependence of σ_{BEC} for various trap geometries. Since the initial phase of a Bose condensate is mapped into its density distribution after ballistic expansion, the quantity σ_{BEC} is a direct measure of the initial phase fluctuations. Note however, that this method reflects the instantaneous phase of the BEC at the time of release and therefore images taken at the same initial conditions can look significantly different. Indeed, we observe a large spread of our experimental data (see Fig. 5). The scatter in these cases is mainly due to the statistical character of the phase fluctuations as well as due to the uncertainties in the temperature determination. For all traps the highest temperature data correspond to values close to T_c ($T \approx 0.9T_c$) which is increasing for tighter confinement. On average the phase fluctuations continuously decrease with falling temperature and get more pronounced with increasing aspect ratio. The reduction of the observed phase fluctuations for lower temperatures is due to both, the reduced excitation spectrum at lower temperature and the increasing number of condensed atoms. Due to the loss of particles caused by evaporation, lowering the temperature reduces the total number of particles but the fraction of condensed atoms relative to the total particle number is increased as shown in Fig. 4. It is not possible to determine a cut-off for the phase fluctuations, rather they decrease until they cannot be resolved below our noise limit. Hence all experiments with BECs at finite temperature in tightly confining elongated potentials will be subject to axial phase fluctuations.

3.4 Evaluation of averaged phase fluctuations

Due to the statistical character of phase fluctuations every experimental realization has a different phase distribution. Therefore, we average the observed standard deviations for a small range of experimental parameters to obtain general information about the phase fluctuations and to compare our measurements to the theoretical prediction. According to Eq. (14) the standard deviation of the fluctuations is expected to depend on the square root of the temperature. This behaviour can not be observed in Fig. 5 since the condensate number changes with temperature. Therefore, we use that equation to scale out the influence of condensate number, trapping potential, and time-of-flight. In figure 6 the measured standard deviations are plotted as function of $T/T_\phi C^2$, where T_ϕ and C (C taken at $x=0$) are calculated from the measured number of condensed atoms, trapping frequencies, and expansion times. The figure shows that all data points fall on an universal square root shaped curve. This means, that our experimental results follow the expected dependence very well.

As a main result, with the direct link of the phase fluctuations in the magnetic trap to the observed density modulations given by Eq. (16), our measurements confirm the predicted behaviour of phase fluctuations in elongated BECs.

As explained above, a precise quantitative comparison needs to take into account a reduced contrast due to the limited experimental resolution and a possible tilt of the detection laser beam with respect to the structures. If we account for a resolution of our imaging system of $\sigma = 3\mu\text{m}$, the predicted standard deviations are about a factor of 2 bigger than the observed deviations. A possible reason might be a small tilt of the detection laser beam. For our parameters a tilt of only 4° reduces the observed modulations by a factor of approximately 2.

Note, that our measurements were performed in elongated geometries but our condensates still were in a 3D-regime in the sense that the chemical potential was greater than the transverse level spacing. Nevertheless, most of our measurements, which exhibit fluctuations well above our noise level, correspond to the regime of quasicondensation in which the phase coherence length is smaller than the condensate size. For instance, for $\lambda = 51$, $T = 0.5T_c$, and $N_0 = 3 \times 10^4$, one obtains $\mu = 3.4\hbar\omega_\rho$ and $l_\phi \approx L/3$.

4 Discussion of alternative methods

In principle, phase fluctuations may be observed by all experiments on BEC which rely on its phase properties. Hence, various methods may be used to study them. We have presented a method which is based on the transfer of phase fluctuations into density modulations after ballistic expansion. A great advantage of our method

is its applicability to very different trap geometries and that the sensitivity depends on the chosen time-of-flight t (see Eq. (16)). In principle for longer t the method becomes more and more sensitive for initial phase fluctuations. On the other hand the decreasing density reduces the signal-to-noise ratio leading to an optimum time-of-flight for given parameters. In our case a time-of-flight of 25 ms allows us to measure phase fluctuations of only $\delta_L^2 \approx \pi/7$. Moreover, time-of-flight methods constitute a standard experimental tool to study properties of BECs. Therefore, understanding the formation of stripes in the density distribution is of great importance. It is instructive to discuss two of the most successful methods used to study the coherence properties of BEC, namely Bragg spectroscopy [10] and interferometry [3], with respect to the measurement of phase fluctuations.

4.1 Bragg spectroscopy

The velocity field of a condensate is proportional to the gradient of its phase. Therefore, phase fluctuations lead to a broadening of the momentum distribution of a trapped condensate which can be measured using Bragg spectroscopy. Since in elongated condensates phase fluctuations are predominantly provided by axial excitations the momentum distribution along the axial direction has to be measured. The average momentum distribution \mathcal{P} is given by the Fourier transform (\mathcal{FT}) of the integrated single-particle correlation function $G(\mathbf{r}_a) \equiv \int d^3r \langle \hat{\psi}^\dagger(\mathbf{r}) \hat{\psi}(\mathbf{r} + \mathbf{r}_a) \rangle$ [27]. Using Eq. (1) and the definition of the phase coherence length we get

$$\begin{aligned} \mathcal{P}(p) &= \mathcal{FT} \left[\exp^{-\frac{|\mathbf{r}_a|}{l_\phi}} \int d^3r \sqrt{n_0(\mathbf{r}) n_0(\mathbf{r} + \mathbf{r}_a)} \right] \\ &= \mathcal{FT} \left[\exp^{-\frac{|\mathbf{r}_a|}{l_\phi}} \right] \star \mathcal{FT} \left[\langle \sqrt{n_0(\mathbf{r}) n_0(\mathbf{r} + \mathbf{r}_a)} \rangle_{\mathbf{r}} \right] \end{aligned}$$

which is a convolution of the Fourier transform of the density distribution and that of a Gaussian with the width of the phase coherence length l_ϕ . Thus, the first term is inversely proportional to l_ϕ , the second inversely proportional to the condensate size. In the absence of phase fluctuations the momentum distribution is limited by the size of the condensate, i. e. , Heisenberg-uncertainty limited. In the regime of quasicondensates where the phase coherence length is smaller than the condensate size, the momentum distribution is dominated by the phase coherence length, thus increasing the momentum width significantly with respect to the Heisenberg limit. However, for a trapped condensate the width of the Bragg resonance is not only determined by this momentum width (Doppler width) but also by the inhomogeneous density distribution, leading to a spatially inhomogeneous mean field-shift of the resonance and therefore broadening it.

We will now briefly estimate the relative contribution of the momentum width and the mean-field width to the

total linewidth of the Bragg resonance. For typical parameters of $N = 10^5$, $w_\rho = 2\pi \times 365$ Hz, $w_x = 2\pi \times 14$ Hz the momentum width resulting from the size of the condensate is $\Delta\nu_{\text{size}} = \sqrt{21/8} \frac{2\hbar k}{2\pi m L} = 57$ Hz, where $k = 2\pi/\lambda$ is the absolute value of the wavevector of the Bragg beams. For these parameters the mean field broadening is $\Delta\nu_{\text{mf}} = \sqrt{8/147} \frac{\mu}{\hbar} = 536$ Hz. Hence the total width of the resonance is $\Delta\nu = \sqrt{\Delta\nu_{\text{momentum}}^2 + \Delta\nu_{\text{mf}}^2} = 539$ Hz. Here, we have taken the expressions for the widths from Ref. [10] and assumed Bragg spectroscopy with counterpropagating beams since this leads to the highest momentum resolution. For a temperature $T = 0.5T_c$ the phase coherence length is, according to Eq. (5), $l_\phi \approx 1.4L$ ($\delta_L^2 \approx \pi/5$). Though this increases the momentum width roughly by a factor of 2, it leads only to a total linewidth of approximately 547 Hz. Thus, the contribution of the momentum width to the total linewidth in this case is less than 2%, making it very difficult to detect. In contrast, our measurements show that the method of ballistic expansion is capable of detecting even such small phase fluctuations.

4.2 Interferometry

Interferometry has been successfully used to study and to characterize the spatial phase of Bose condensates. Therefore, it is natural to consider possibilities to extend such methods to determine the amount of phase fluctuations in trapped atomic gases. In analogy to classical optics, there are several methods to use interferometry to determine the coherence properties of a condensate wave function. These include, e.g., the double slit experiment with outcoupled atom laser beams [4] and interference between two overlapping condensates [2]. In the latter case, two spatially separated condensates were prepared independently and their interference was measured after a ballistic expansion. The results indicated a flat phase distribution of the initial wavefunction for the experimental parameters used in those measurements. In general, interferometric measurements rely on the superposition of two wavefunctions and the interpretation of the resulting fringe pattern. The existence of a randomly fluctuating phase as shown in Fig.1 complicates the interpretation.

To visualize possible experimental results, let us first consider the following situation. A given phase fluctuating condensate is coherently split in two equal parts giving one of them a small additional velocity. Absorption images taken of the overlapping condensates will show interference fringes. For condensates with a constant phase the images would show regularly spaced lines. However due to the phase fluctuations these lines will be shifted according to the relative fluctuating phase, leading to a random, spatially varying fringe spacing. Similar to the ballistic expansion measurements these images

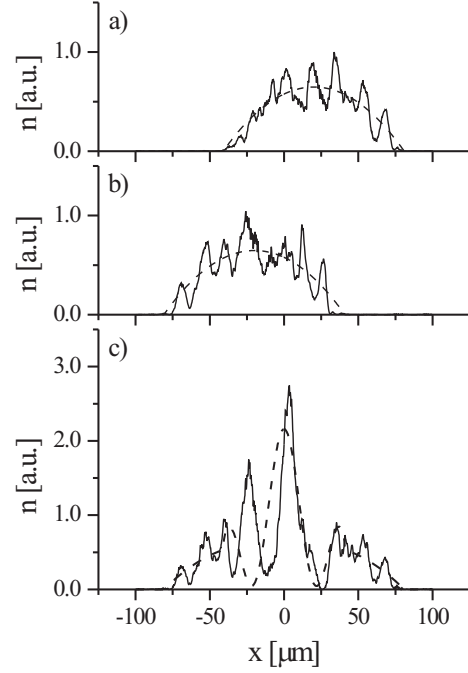


Fig. 7 (a, b) Examples of independently calculated density distributions of phase fluctuating condensates (solid line) for $\omega_\rho = 2\pi \times 715$ Hz, $\omega_x = 2\pi \times 14$ Hz, $N = 5 \times 10^4$ and $T = 0.6T_c$ compared to that of a condensate at $T = 0$ (dashed line) for a time-of-flight of 15 ms. (c) Interference pattern of the superposition of the condensates shown in a) and b) with a relative displacement of $\Delta x = 40 \mu\text{m}$.

will be different from shot to shot and allow only for a statistical evaluation.

So far most interferometric measurements with BECs have been performed after a ballistic expansion. An additional complication arises in these experiments, since both density and phase of the sample evolve during the free expansion time. Let us assume that two independent quasicondensates are brought to partial overlap after a time-of-flight with zero relative velocity (using e. g. Bragg pulses [5, 7, 8]). At this point modulations have appeared in the density distribution and the phase has evolved from its initial random pattern. Both parts now contribute to the formation of stripes in the interference pattern, making a direct interpretation difficult.

Figure 7 shows an example of an expected absorption image for our experimental conditions. Both wavefunctions Ψ_1 and Ψ_2 of the phase fluctuating condensates were calculated after a time-of-flight of 15 ms using the GP equation. The interference pattern is given by $|\Psi_1(x) + \Psi_2(x + \Delta x)|^2$, where Δx is the displacement of the two quasicondensates. Fig. 7 a) and b) show the density distribution of the two quasicondensates (solid line) displaced by $\Delta x = 40 \mu\text{m} \approx 2l_\phi$ in comparison with the Thomas-Fermi distribution of a condensate at $T = 0$ (dashed line). Note, that the structures shown there are

the density modulations due to the phase fluctuations only. The resulting interference pattern of these two independent condensates is then displayed in Fig. 7 c). At $T = 0$ the interference pattern is due to the small axial expansion velocity, which leads to a quadratic phase. In the case of the quasicondensates the profile looks considerably different, i. e. the phase fluctuations lead to a significant change of the experimental outcome. Due to the difficult interpretation of the density distribution, interferometric methods together with a long expansion time are not suited very well for analysis of phase fluctuations. However, interferometric methods that work with a short expansion time or even with trapped condensates might be very useful for visualization of the spatial profile of phase fluctuations. Such methods might include, e.g. preparation of two independent quasicondensates with a small vertical separation. After a short time-of-flight the radial expansion of the clouds leads to their partial superposition, and consequently interference in the overlap region. In the case of constant relative phase in the axial direction horizontal stripes appear in the overlap region. Due to the phase fluctuations the relative phase can, however, change as a function of axial position, which is seen as bending of the interference fringes in the vertical direction. Therefore, the relative phase profile of the clouds can be imaged by measuring the shape of the interference fringes.

5 Conclusion

We have presented detailed experimental and theoretical studies of phase fluctuations in the equilibrium state of BECs. A strong dependence on the trap geometry and temperature has been found in agreement with the theoretical prediction. We have shown that phase fluctuations are a general property of elongated condensates. By measuring the phase fluctuations and comparing the temperature with T_ϕ we have demonstrated instances, where the phase coherence length was smaller than the axial size of the condensate, i.e. the initial cloud was a quasicondensate. Our results set severe limitations on applications of BECs in interferometric measurements, and for guided atom laser beams. Our experimental method combined with the theoretical analysis provides a method of BEC thermometry. Further studies of the effect of phase fluctuations, e. g. on the superfluid properties, will give additional insight to the behaviour of degenerate quantum gases at finite temperature.

This work is supported by the *Deutsche Forschungsgemeinschaft* within the SFB 407 and the Schwerpunktprogramm "Wechselwirkungen ultrakalter atomarer und molekularer Gase", and the European Science Foundation (ESF) within the BEC2000+ programme. DSP acknowledges support from the Alexander von Humboldt Foundation, from the Dutch Foundations NWO and FOM, and from the Russian Foundation for Basic Research.

References

1. See e.g. F. Dalfovo, S. Giorgini, L. P. Pitaevskii, and S. Stringari, *Rev. Mod. Phys.* **71**, 463 (1999).
2. M. R. Andrews, C. G. Townsend, H.-J. Miesner, D. S. Durfee, D. M. Kurn, and W. Ketterle, *Science* **275**, 637 (1997).
3. E. W. Hagley, L. Deng, M. Kozuma, M. Trippenbach, Y. B. Band, M. Edwards, M. R. Doery, P. S. Julienne, K. Helmerson, S. L. Rolston, and W. D. Phillips, *Phys. Rev. Lett.* **83**, 3112 (1999).
4. I. Bloch, T. W. Hänsch, and T. Esslinger, *Nature* **403**, 166 (2000).
5. J. E. Simsarian, J. Denschlag, Mark Edwards, Charles W. Clark, L. Deng, E. W. Hagley, K. Helmerson, S. L. Rolston, and W. D. Phillips, *Phys. Rev. Lett.* **85**, 2040 (2000).
6. D. S. Hall, M. R. Matthews, C. E. Wieman, and E.A. Cornell, *Phys. Rev. Lett.* **81**, 1543 (1998).
7. Y. Torii, Y. Suzuki, M. Kozuma, T. Sugiura, T. Kuga, L. Deng, and E. W. Hagley, *Phys. Rev. A* **61**, R041602 (2000).
8. K. Bongs, S. Burger, S. Dettmer, D. Hellweg, J. Arlt, W. Ertmer, and K. Sengstock, *Phys. Rev. A* **63**, R31602 (2000).
9. M.-O. Mewes, M. R. Andrews, D. M. Kurn, D. S. Durfee, C. G. Townsend, and W. Ketterle, *Phys. Rev. Lett.* **78**, 582 (1997); B. P. Anderson, and M. A. Kasevich, *Science* **282**, 1686 (1998); E. W. Hagley, L. Deng, M. Kozuma, J. Wen, K. Helmerson, S.L. Rolston, and W. D. Phillips, *Science* **283**, 1706 (1999); I. Bloch, T. W. Hänsch, and T. Esslinger, *Phys. Rev. Lett.* **82**, 3008 (1999); F. Gerbier, P. Bouyer, and A. Aspect, *Phys. Rev. Lett.* **86**, 4729 (2001).
10. J. Stenger, S. Inouye, A. P. Chikkatur, D. M. Stamper-Kurn, D. E. Pritchard, and W. Ketterle, *Phys. Rev. Lett.* **82**, 4569 (1999).
11. Yu. Kagan, in *Bose-Einstein Condensation*, edited by A. Griffin, D. W. Snoke, and S. Stringari (Cambridge University Press, Cambridge, 1995), p. 202–225; and references therein.
12. D. S. Petrov, G. V. Shlyapnikov, and J. T. M. Walraven, *Phys. Rev. Lett.* **85**, 3745 (2000).
13. D. S. Petrov, M. Holzmann, and G. V. Shlyapnikov, *Phys. Rev. Lett.* **84**, 2551 (2000).
14. Yu. Kagan, V. A. Kashurnikov, A. V. Krasavin, N. V. Prokof'ev, and B.V. Svistunov, *Phys. Rev. A* **61**, 43608 (2000); N. J. van Druten, and W. Ketterle, *Phys. Rev. Lett.* **79**, 549 (1997); H. Monien, M. Linn, and N. Elstner, *Phys. Rev. A* **58**, R3395 (1998); M. Olshanii, *Phys. Rev. Lett.* **81**, 938 (1998); and references therein.
15. A. I. Safonov, S. A. Vasilyev, I. S. Yasn timer, I. I. Lukashevich, and S. Jaakkola, *Phys. Rev. Lett.* **81**, 4545 (1998).
16. A. Görlitz, J. M. Vogels, A. E. Leanhardt, C. Raman, T. L. Gustavson, J. R. Abo-Shaeer, A. P. Chikkatur, S. Gupta, S. Inouye, T. P. Rosenband, D. E. Pritchard, and W. Ketterle, *cond-mat/0104549*.
17. F. Schreck, L. Khaykovich, K. L. Corwin, G. Ferrari, T. Bourdel, J. Cubizolles, and C. Salomon, *cond-mat/0107442*.
18. D. S. Petrov, G. V. Shlyapnikov, and J. T. M. Walraven, *Phys. Rev. Lett.* **87**, 050404 (2001).
19. S. Dettmer, D. Hellweg, P. Ryytty, J. J. Arlt, W. Ertmer, K. Sengstock, D. S. Petrov, G. V. Shlyapnikov, H. Kreutzmann, L. Santos, and M. Lewenstein, *cond-mat/0105525*.

- 20. J. Reichel, and T. W. Hänsch, private communication;
C. Zimmermann, private communication.
- 21. S. Stringari, Phys. Rev. A **58**, 2385 (1998).
- 22. V. N. Popov, *Functional Integrals in Quantum Field Theory and Statistical Physics*, (D. Reidel Pub., Dordrecht, 1983).
- 23. S. I. Shevchenko, Sov. J. Low Temp. Phys. **18**, 223 (1992).
- 24. Yu. Kagan, E. L. Surkov, and G. V. Shlyapnikov, Phys. Rev. A **54**, R1753 (1996); Y. Castin and R. Dum, Phys. Rev. Lett. **77**, 5315 (1996).
- 25. K. Bongs, S. Burger, G. Birkl, K. Sengstock, W. Ertmer, K. Rzażewski, A. Sanpera, and M. Lewenstein, Phys. Rev. Lett. **83**, 3577 (1999).
- 26. S. Burger, K. Bongs, S. Dettmer, W. Ertmer, K. Sengstock, A. Sanpera, G. V. Shlyapnikov, and M. Lewenstein, Phys. Rev. Lett. **83**, 5198 (1999).
- 27. See for example C. Cohen-Tannoudji, Lecture notes of the Euroschool Bose-Einstein Condensates and Atom lasers, Cargese, France (2000).